

# Efficient parametric generation in a nonlinear photonic crystal pumped by a dual beam

E. BRAMBILLA,<sup>1</sup> AND A. GATTI<sup>2,1</sup>

<sup>1</sup> *Dipartimento di Scienza e Alta Tecnologia dell' Università dell'Insubria, Via Valleggio 11, Como, Italy*

<sup>2</sup> *Istituto di Fotonica e Nanotecnologie del CNR, Piazza Leonardo Da Vinci 32, Milano, Italy*

\*[opex@osa.org](mailto:opex@osa.org)

**Abstract:** We investigate parametric down-conversion in a hexagonally poled nonlinear photonic crystal, pumped by a dual pump with a transverse modulation that matches the periodicity of the  $\chi^{(2)}$  nonlinear grating. A peculiar feature of this resonant configuration is that the two pumps simultaneously generate photon pairs over an entire branch of modes, via quasi-phasematching with both fundamental vectors of the reciprocal lattice of the nonlinearity. The parametric gain of these modes depends thus coherently on the sum of the two pump amplitudes and can be controlled by varying their relative intensities and phases. We find that a significant enhancement of the source conversion efficiency, comparable to that of one-dimensionally poled crystals, can be achieved by a dual symmetric pump. We also show how the four-mode coupling arising among shared modes at resonance can be tailored by changing the dual pump parameters.

© 2021 Optical Society of America under the terms of the [OSA Open Access Publishing Agreement](#)

## Introduction

Since their proposal by Berger [1] and their first realization [2],  $\chi^{(2)}$  nonlinear photonic crystals (NPC) with a two-dimensional poling pattern have attracted great interest due to their potential applications in nonlinear optics [3–9], as well as in quantum optics for the generation and engineering of entangled states [10–15]. Considering parametric down-conversion (PDC) from an intense pump beam into twin photons or twin beams of lower frequencies, the vectors of the 2D reciprocal lattice associated to the nonlinear grating indeed offer multiple quasi-phasematching (QPM) possibilities not encountered in more conventional one-dimensional structures. Specifically, the source emission spectrum is characterized by special points, the so called "shared modes" lying at the interception of different QPM branches associated to non collinear lattice vectors [15–19]. In the stimulated regime of PDC, these shared modes are cross-seeded by two coupled modes simultaneously, with a significant enhancement of the parametric gain [15, 16]. These three-mode interaction processes involving the shared modes appear therefore in the source far field as localized bright spots against a more diffused background coming from standard two-mode PDC.

A recent analysis for a hexagonally poled crystal [14, 15] demonstrated a peculiar spatial resonance, reached by tilting the pump angle till its phase modulation matches the periodicity of the poling pattern: this enforces a transition from three- to four-mode entanglement among shared modes, the latter being dominated by the Golden Ratio of the segment  $\phi = (1 + \sqrt{5})/2$ . In the stimulated PDC regime, a sudden boost of the intensity of shared modes takes place as the pump incidence angle is tuned to resonance [15]. The quantum aspects of the underlying entangled state have been investigated in [14].

In this work we shall explore the possibility of modulating the intensity of the pump beam in the transverse plane, rather than only its phase, through the use of a dual pump. Coherent coupling in  $\chi^{(2)}$  materials via dual pumping has been investigated both in a bulk crystal [20], and in a one-dimensionally poled QPM structure [21], with the realization of self-diffraction in the first case, and resonant cascaded four-wave mixing in the second case.

In the 2D nonlinear photonics crystal we consider here, the addition of a second pump

wave increases the complexity of the source spectrum, due to the increased QPM opportunities involving the two pump modes and the two vectors of the hexagonal reciprocal lattice. We shall focus on the condition of spatial resonance between the pump modulation and the nonlinear pattern, and demonstrate some unique features not encountered in the conventional single pump configuration.

A first noticeable feature is the existence of an entire branch of modes (a 3D surface in the Fourier domain) in which photon pairs are down-converted from both pumps simultaneously, quasi-phase matched by two fundamental vectors of the reciprocal lattice. We shall show that the parametric gain of this QPM branch depends on the coherent sum of the two pump amplitudes  $|\alpha_1 + \alpha_2|$  and can be controlled by varying their relative intensities and phases. In particular, the use of a dual symmetrical pump ( $\alpha_1 = \alpha_2$ ) leads to a substantial increase of the gain compared to a single pump beam of the same energy. As a result, the dual pump configuration may in principle bring the source conversion efficiency close to the level of 1D poled crystals of the same material, compensating at least partially for the lower effective nonlinear coefficients associated to two-dimensional poling patterns [22].

We also show that a dual pumping allows a control over the four-mode processes characterizing the spatial resonance. Maximum enhancement of the shared mode intensity is obtained with two symmetric pumps, while the four-mode coupling degenerates into two independent two-mode processes of reduced gain for anti-symmetric pumps ( $\alpha_2 = -\alpha_1$ ). A dual pump with controlled relative phases and intensities can therefore be used to tailor the multimode coupling among shared modes and, in the quantum domain, to engineer interesting quantum states, which will be the subject of a related investigation [23].

## 1. The model

Our description is based on a model similar to that in [14]. Even if our analysis may apply to various configurations, we focus here on degenerate down-conversion around  $\lambda_s = 1064$  nm from a pump at  $\lambda_p = 532$  nm, taking place in a hexagonally poled Lithium Tantalate ( $\text{LiTaO}_3$ ) slab similar to the one in [10].

Figure 1 shows the arrangement: the  $\chi^{(2)}$  crystal is hexagonally poled in the  $(x, z)$  plane orthogonal to the crystal optical axis (the crystal optical axis corresponds to the  $y$ -axis of the reference frame used in this work, shown in Fig. 1a). We consider type 0 phase-matching  $e \rightarrow e, e$ , where both the pump and the down-converted field are extraordinarily polarized along the optical axis, and propagate mainly in the  $(x, z)$  plane, forming small angles with a mean propagation direction (the  $z$ -axis in the figure). In particular the pump beam consists of two waves slightly and symmetrically tilted with respect to the  $z$ -axis, giving rise to a spatial transverse modulation of the pumping of the medium. When the transverse modulation of the pump matches the one of the nonlinear pattern (Fig. 1(b)), a condition of spatial resonance is achieved. In such conditions, quasi phase-matching at the degenerate wavelength  $2\lambda_p$  is achieved when the – poling period of the two-dimensional pattern is  $\Lambda = \frac{2\pi}{G_z} = 7.782 \mu\text{m}$  at a temperature of  $85^\circ\text{C}$ , according to the Sellmeier relations in [24]. These are the conditions chosen for the numerical simulations of the system that will be shown in the following.

The two-dimensional hexagonal pattern of the nonlinearity is described by keeping only the leading order terms of the Fourier expansion of the nonlinear-susceptibility  $d(x, z)$  [1]. Denoting with  $\vec{G}_1 = -G_x\vec{e}_x - G_z\vec{e}_z$  and  $\vec{G}_2 = +G_x\vec{e}_x - G_z\vec{e}_z$  the two fundamental vectors of the reciprocal lattice which provide quasi-phase matching, we have accordingly

$$d(x, z) \simeq e^{-iG_z z} [d_{01}e^{-iG_x x} + d_{10}e^{iG_x x}] = 2d_{01}e^{-iG_z z} \cos(G_x x) \quad (1)$$

Considering e.g. inversion domains shaped as discs of radius  $R = 0.28\Lambda$  (Fig. 2(a)), one has  $d_{01} = d_{10} = 0.32d_{eff}$  [22],  $d_{eff}$  denoting the effective nonlinear susceptibility of the  $\chi^{(2)}$  material.

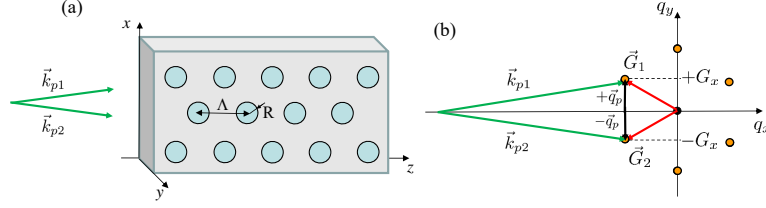


Fig. 1. a) Hexagonally poled  $\chi^{(2)}$  crystal pumped by two waves, symmetrically tilted with respect to the  $z$ -axis. b) A spatial resonance is achieved by matching the pump transverse wave-vectors  $\pm \vec{q}_p$  with the transverse components  $\pm \vec{G}_x$  of the lattice vectors  $\vec{G}_1$  and  $\vec{G}_2$ .

In the degenerate type 0 case, the signal and idler modes belong to the same wave-packet of central frequency  $\omega_s = \omega_p/2$ . The signal and pump envelope operators, denoted by  $\hat{A}_s$  and  $\hat{A}_p$  respectively, satisfy the following coupled propagation equations in the Fourier domain (see [14] and [25, 26])

$$\frac{\partial}{\partial z} \hat{A}_s(\vec{w}_s, z) = \chi \int \frac{d^3 \vec{w}_p}{(2\pi)^{\frac{3}{2}}} \hat{A}_p(\vec{w}_p, z) \left[ \hat{A}_s^\dagger(\vec{w}_p - \vec{w}_s - \vec{\mathcal{G}}_x, z) e^{-i\mathcal{D}(\vec{w}_s, \vec{w}_p - \vec{w}_s - \vec{\mathcal{G}}_x)z} + \hat{A}_s^\dagger(\vec{w}_p - \vec{w}_s + \vec{\mathcal{G}}_x, z) e^{-i\mathcal{D}(\vec{w}_s, \vec{w}_p - \vec{w}_s + \vec{\mathcal{G}}_x)z} \right] \quad (2a)$$

$$\frac{\partial}{\partial z} \hat{A}_p(\vec{w}_p, z) = -\frac{\chi}{2} \int \frac{d^3 \vec{w}_s}{(2\pi)^{\frac{3}{2}}} \hat{A}_s(\vec{w}_s, z) \left[ \hat{A}_s(\vec{w}_p - \vec{w}_s - \vec{\mathcal{G}}_x, z) e^{i\mathcal{D}(\vec{w}_s, \vec{w}_p - \vec{w}_s - \vec{\mathcal{G}}_x)z} + \hat{A}_s(\vec{w}_p - \vec{w}_s + \vec{\mathcal{G}}_x, z) e^{i\mathcal{D}(\vec{w}_s, \vec{w}_p - \vec{w}_s + \vec{\mathcal{G}}_x)z} \right] \quad (2b)$$

where  $\vec{w}_j = (\vec{q}, \Omega)$ ,  $j = s, p$ , denotes the coordinate in the 3D Fourier space of the  $j$ -th field, with  $\vec{q} = (q_x, q_y)$  being the transverse component of the wave-vector, and  $\Omega$  the offset frequency from the corresponding carrier frequencies  $\omega_s$  and  $\omega_p = 2\omega_s$ .  $\vec{\mathcal{G}}_x = (G_x, 0, 0)$  is a short-hand notation for the  $x$ -component of the reciprocal lattice vector in the 3D Fourier space, and  $\chi \simeq d_{01} \sqrt{\frac{\hbar \omega_p \omega_s^2}{8\epsilon_0 c^3 n_p n_s^2}}$ . The two terms at r.h.s of Eqs.(2b) describe all the possible three-photon processes  $\vec{w}_p \leftrightarrow \vec{w}_s, \vec{w}_i = \vec{w}_p - \vec{w}_s \pm \vec{\mathcal{G}}_x$  mediated by the lattice vectors  $\vec{G}_1$  and  $\vec{G}_2$  respectively. Notice that for a given pump mode  $\vec{w}_p = (\vec{q}_p, \Omega_p)$ , the energy and transverse momentum conservation imply that  $\vec{w}_s + \vec{w}_i = \vec{w}_p \pm \vec{\mathcal{G}}_x$ , i.e.  $\Omega_s + \Omega_i = \Omega_p$ , and  $\vec{q}_s + \vec{q}_i = \vec{q}_p \pm \vec{G}_x \vec{e}_x$ , the latter condition deriving from the simplifying assumption that the crystal is indefinitely extended in the transverse plane. On the other hand, since we are considering a crystal of finite length  $l_c$  along the  $z$ -direction, the longitudinal momentum conservation is less stringent, and is expressed by the phase-matching functions appearing at the r.h.s. of Eqs. (2a), (2b)

$$\mathcal{D}(\vec{w}_s, \vec{w}_p - \vec{w}_s \pm \vec{\mathcal{G}}_x) = [k_{sz}(\vec{w}_s) + k_{sz}(\vec{w}_p - \vec{w}_s \pm \vec{\mathcal{G}}_x) - k_{pz}(\vec{w}_p) + G_z], \quad (3)$$

where  $k_{jz}(\vec{w}_j) = \sqrt{k_j^2(\vec{w}_j) - q^2}$  is the  $z$ -components of the wave-vectors associated to mode  $\vec{w}_j$ , the wave number  $k_j(\vec{w}_j) = \frac{\omega_j + \Omega}{c} n_j(\vec{w}_j)$  being determined by the linear dispersion relation of the  $j$ -th wave in the medium. Notice that since all the fields are extraordinarily polarized, their refractive index in principle depends on the propagation direction through  $q_y$ :  $n_j(\vec{w}_j) = n_e(\omega_j + \Omega_j, q_y)$ . However, spatial walk-off is negligible since the fields propagate nearly at  $\pi/2$  from the optical axis, and more in general Lithium Tantalate is characterized by a very small birefringence [27]. Thus we shall neglect the crystal anisotropy both in analytical calculations and in the numerical

simulations, letting  $n_j(\vec{w}_j) = n_e(\omega_j + \Omega, q_y = 0)$ , where  $n_e$  is the crystal extraordinary refractive index in the lattice plane.

## 2. Dual plane-wave pump

In view of obtaining analytical results, we consider the parametric limit where the pump field in Eqs. (2) is treated as a classical coherent field undergoing negligible depletion during propagation. With respect to the pure phase modulation discussed in [14, 15], where a spatial resonance was realized by tilting a single pump wave, we assume here that the pump consists of two monochromatic plane-waves of frequency  $\omega_p$ , symmetrically tilted from the  $z$ -axis in the lattice plane, as shown in Fig. 1. Thus, our analysis includes the possibility of an intensity modulation of the pump. Denoting as  $\vec{q}_{0p} = \pm q_{0p} \vec{e}_x$  the pump transverse wave-vectors, in the direct space  $A_p(\vec{x}, t) = \alpha_1 e^{iq_{0p}x} + \alpha_2 e^{-iq_{0p}x}$ , while in the Fourier domain

$$\begin{aligned} A_p(\vec{q}, \Omega_p) &= \int \frac{dt}{\sqrt{2\pi}} \int \frac{d\vec{x}}{2\pi} e^{i\Omega t - i\vec{q} \cdot \vec{x}} A_p(\vec{x}, t) \\ &= (2\pi)^{3/2} \delta(\Omega) \delta(q_y) [\alpha_1 \delta(q_x - q_{0p}) + \alpha_2 \delta(q_x + q_{0p})] \end{aligned} \quad (4)$$

Quasi-phases matching is achieved for signal modes belonging to one of the four distinct QPM surfaces in the  $\vec{w}_s$ -space:

$$\Sigma_{11} : \mathcal{D}(\vec{w}_s, \vec{w}_{0p} - \vec{w}_s + \vec{\mathcal{G}}_x) = 0 \quad [\vec{q}_s + \vec{q}_i = (q_{0p} + G_x) \vec{e}_x] \quad (5a)$$

$$\Sigma_{12} : \mathcal{D}(\vec{w}_s, \vec{w}_{0p} - \vec{w}_s - \vec{\mathcal{G}}_x) = 0 \quad [\vec{q}_s + \vec{q}_i = (q_{0p} - G_x) \vec{e}_x] \quad (5b)$$

$$\Sigma_{21} : \mathcal{D}(\vec{w}_s, -\vec{w}_{0p} - \vec{w}_s + \vec{\mathcal{G}}_x) = 0 \quad [\vec{q}_s + \vec{q}_i = -(q_{0p} - G_x) \vec{e}_x] \quad (5c)$$

$$\Sigma_{22} : \mathcal{D}(\vec{w}_s, -\vec{w}_{0p} - \vec{w}_s - \vec{\mathcal{G}}_x) = 0 \quad [\vec{q}_s + \vec{q}_i = -(q_{0p} + G_x) \vec{e}_x] \quad (5d)$$

where  $\pm \vec{w}_{0p} = (\pm q_{0p}, q_y = 0, \Omega = 0)$  denote the 3D Fourier components of the two pump modes and the relations within the graph parentheses give the transverse momentum conservation associated to each QPM surface. We focus here on the condition of *spatial resonance*, obtained by matching the pump transverse modulation to that of the nonlinear lattice, i.e. setting

$$q_{0p} = G_x \quad \rightarrow \quad A_p(z, \vec{x}, t) = \alpha_1 e^{iG_x x} + \alpha_2 e^{-iG_x x} \quad (6)$$

In this case  $\Sigma_{12}$  and  $\Sigma_{21}$  merge into the single surface

$$\Sigma_{12}, \Sigma_{21} \rightarrow \Sigma_0 : \quad \mathcal{D}(\vec{w}_s, -\vec{w}_s) = 0 \quad (7)$$

It is important to stress that photon pairs belonging to  $\Sigma_0$  originate simultaneously from both pump modes and are quasi-phase matched by both vectors  $\vec{\mathcal{G}}_1$  and  $\vec{\mathcal{G}}_2$  of the grating of the nonlinearity. On the other hand, the two other QPM surfaces

$$\Sigma_{11} : \mathcal{D}(\vec{w}_s, -\vec{w}_s + 2\vec{\mathcal{G}}_x) = 0, \quad (8)$$

$$\Sigma_{22} : \mathcal{D}(\vec{w}_s, -\vec{w}_s - 2\vec{\mathcal{G}}_x) = 0 \quad (9)$$

are populated only by down-conversion either from pump 1 with the contribution of the lattice vector  $\vec{\mathcal{G}}_1$  (photon pairs appearing on  $\Sigma_{11}$ ), or from pump 2 mediated by the lattice vector  $\vec{\mathcal{G}}_2$  (photon pairs appearing on  $\Sigma_{22}$ ).

Substituting Eq. (4) into Eq. (2a), one obtains the following propagation equation

$$\begin{aligned} \frac{\partial \hat{A}_s}{\partial z}(\vec{w}_s) &= (g_1 + g_2) \hat{A}_s^\dagger(-\vec{w}_s) e^{-i\mathcal{D}(\vec{w}_s, -\vec{w}_s)z} + g_1 \hat{A}_s^\dagger(-\vec{w}_s + 2\vec{\mathcal{G}}_x) e^{-i\mathcal{D}(\vec{w}_s, -\vec{w}_s + 2\vec{\mathcal{G}}_x)z} \\ &\quad + g_2 \hat{A}_s^\dagger(-\vec{w}_s - 2\vec{\mathcal{G}}_x) e^{-i\mathcal{D}(\vec{w}_s, -\vec{w}_s - 2\vec{\mathcal{G}}_x)z} \end{aligned} \quad (10)$$

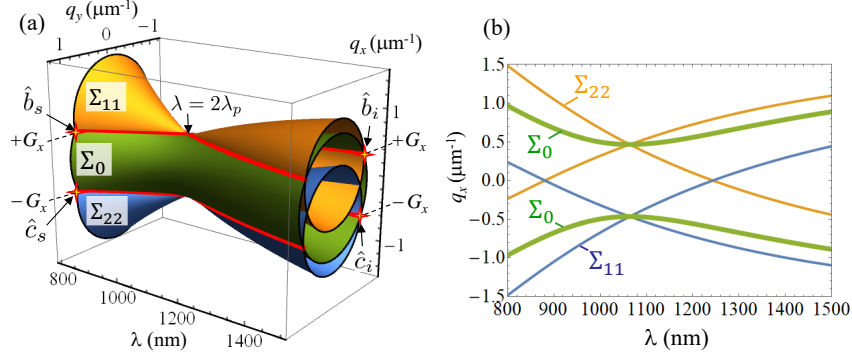


Fig. 2. Quasi phase-matching in a hexagonally poled LiTaO<sub>3</sub> crystal pumped at 532nm by a dual pump at spatial resonance with the lattice:  $q_{0p}\vec{e}_x = G_x\vec{e}_x$ , with  $G_x = 2\pi/(\sqrt{3}\Lambda) = 0.466\mu\text{m}^{-1}$ . (a) QPM surfaces in the 3D Fourier space, and (b) its section at  $q_y = 0$ .

where the complex parameters  $g_1 = \chi\alpha_1$  and  $g_2 = \chi\alpha_2$  represent the parametric gain per unit length associated to each pump mode. The first term at r.h.s. of Eq. (10), proportional to the sum of the two pump amplitudes  $\alpha_1 + \alpha_2$ , account for PDC processes taking place on the QPM surface  $\Sigma_0$ , while the last two terms are associated to the QPM surfaces  $\Sigma_{11}$  and  $\Sigma_{22}$  respectively. The propagation equation (10) for a given mode  $\vec{w}_s$  has to be considered together with the propagation equations for the three coupled modes  $\hat{A}_s(-\vec{w}_s)$  and  $\hat{A}_s(-\vec{w}_s \pm 2\vec{G}_x)$  appearing at its right hand side, obtaining in principle an infinite chain of coupled equations for modes of all harmonic orders  $\pm\vec{w}_s + n\vec{G}_x$  (see [14] for details). However, by inspecting which modes are effectively phase-matched to the considered signal mode  $\vec{w}_s$ , the chain can be truncated to finite sets of equations, obtaining thereby coupled equations for either 2-mode or 4-mode processes that will be discussed in the next sections.

Figure 2 shows an example of the three QPM surfaces in the 3D Fourier space of the signal modes, obtained by numerically solving Eqs. (7)-(9) by means of the Sellmeier formula reported in [24]. The period of the poling pattern is chosen to achieve QPM at degeneracy for the shared signal modes emitted at  $q_x = \pm G_x$ ,  $q_y = 0$ , as explained in App. A [see Eq. (7)]. In the same appendix we derive general expressions for these QPM surfaces valid within the paraxial approximation and not too far from degeneracy. In particular, for the chosen crystal parameters,  $\Sigma_{11}$  and  $\Sigma_{22}$  are well approximated by the two biconical surfaces given in Eqs. (8) and (9), having their vertexes at  $\pm G_x\vec{e}_x$ . Their projections onto the plane  $(\lambda, q_x)$  (Fig. 2(b)), are two X-shaped curves symmetrically displaced along the  $q_x$  axis, describing parametric emission collinear with each of the two tilted pumps. Within the same approximations,  $\Sigma_0$  has equation  $|\vec{q}_s| \approx (G_x^2 + k_s k_s'' \Omega_s^2)^{1/2}$ , corresponding approximately to a wide tube, centered at  $\vec{q} = 0$ , describing noncollinear PDC emission at an angle  $\theta \approx G_x/k_s$  around the  $z$ -axis. Notice that the  $\Sigma_0$  surface includes the vertexes of the two cones.

### 2.1. Two-mode processes

Let us consider signal modes for which only one of the three QPM conditions described by Eqs. (7)-(9) is satisfied. These represent the vast majority of modes, with the remarkable exception of modes lying at the intersections of two distinct QPM surfaces, which will be analysed in the next section. Eq. (10) reduces then to standard two-mode parametric equations of the form:

$$\frac{\partial \hat{A}_s}{\partial z}(\vec{w}_s) = \gamma \bar{g} e^{i\phi_1} \hat{A}_s^\dagger(\vec{w}_i) e^{-i\mathcal{D}(\vec{w}_s, \vec{w}_i)z} \quad (11a)$$

$$\frac{\partial \hat{A}_s}{\partial z}(\vec{w}_i) = \gamma \bar{g} e^{i\phi_1} \hat{A}_s^\dagger(\vec{w}_s) e^{-i\mathcal{D}(\vec{w}_s, \vec{w}_i)z} \quad (11b)$$

where  $\vec{w}_i = -\vec{w}_s$  (for modes on the surface  $\Sigma_0$ ) or  $\vec{w}_i = -\vec{w}_s \pm 2\vec{\mathcal{G}}_x$  (on the surfaces  $\Sigma_{11}, \Sigma_{22}$ ), represent the twin idler mode coupled to  $\vec{w}_s$ . Simple inspection of the different terms at the r.h.s. of Eq. (10) allows to determine how the gain of these 2-modes processes compares to the gain from a single pump mode with the same overall intensity  $|\alpha|^2 = |\alpha_1|^2 + |\alpha_2|^2$ . To this end, we set

$$\bar{g} = \sqrt{|g_1|^2 + |g_2|^2} \quad (12)$$

representing the gain one would have by concentrating all the energy in a single pump. According to the standard solution of the parametric equations (11) the number of photons of the phase-matched modes on each QPM surface grows as  $N \propto \sinh^2(|\gamma|\bar{g}z)$  where, by introducing the complex parameter  $r = \frac{g_2}{g_1}$  (without loosing generality we assume that pump 1 is always present, and that  $|g_2/g_1| \leq 1$ ),

$$\gamma = \begin{cases} \frac{g_1 + g_2}{\bar{g}} = \frac{1+r}{\sqrt{1+|r|^2}} & \Sigma_0 \\ \frac{g_1}{\bar{g}} = \frac{1}{\sqrt{1+|r|^2}} & \Sigma_{11} \\ \frac{g_2}{\bar{g}} = \frac{r}{\sqrt{1+|r|^2}} & \Sigma_{22} \end{cases} \quad (13)$$

A striking feature of the spatial resonance (6) is that the parametric gain of modes belonging to the two-fold degenerate surface  $\Sigma_0$  can be controlled by varying the relative intensities and phases of the two tilted pumps. In particular

**i)** Maximum gain on  $\Sigma_0$  is achieved when the two pumps have the same intensity and phase ( $r = 1$  in Fig. 3(b) and 3(e)): this symmetric configuration provides a gain enhancement by a factor  $\gamma = \sqrt{2}$  with respect to the use of a single pump of equivalent intensity. In the stimulated regime  $\bar{g}z > 1$ , this leads to a huge increase of the intensities of the  $\Sigma_0$  modes, as clearly shown by the results in Fig. 4: e.g. in Fig4(a) for  $\bar{g}z = 4$  the  $\Sigma_0$  modes are roughly 30 times more intense when a dual pump is used instead of a single pump. (notice also the different scales of Fig. 3(a) and 3(b)). We stress that this gain enhancement affects also the PDC emission in the spontaneous regime  $\bar{g}z \ll 1$ , in which splitting the available energy into a dual pump doubles the intensity of  $\Sigma_0$ . This occurs because the resonant structure of the pump coherently couples the processes arising from the vectors  $\vec{G}_1$  and  $\vec{G}_2$  of the nonlinear pattern. Thus the use of a dual pump at resonance brings a net increase of the efficiency of parametric generation in photonic crystals, over a whole surface of QPM modes. This is quite different from typical configurations of PDC in nonlinear photonic crystals involving a single pump wave, where shared modes appear as isolated hot spots at the geometrical intersection of different QPM branches [15, 16]. Conversely, the gain on the side branches  $\Sigma_{11}$  and  $\Sigma_{22}$  is reduced by a factor  $\sqrt{2}$ .

**ii)** The  $\Sigma_0$ -modes can be switched off by taking two antisymmetric pumps, with the same intensity and a  $\pi$  phase difference (case  $r = -1$  shown in Fig. 3(c) and 3(f)). Notice that in this case the overall efficiency of quasi-phase-matching with the first order vector of the nonlinear grating is greatly reduced, so that one should consider also the contribution from higher order harmonics of the grating. The relative weight of those secondary PDC processes is however strongly dependent on the motif characterizing the poling grating and will not be discussed in this work.

**iii)** For a single pump, corresponding to a pure phase modulation, the  $\Sigma_0$  and  $\Sigma_{11}$  modes grow with the same gain  $\bar{g}$  and have the same intensity ( $r = 0$  case in Fig. 3(a) and 3(d)). Clearly the

$\Sigma_{22}$  modes are in the vacuum state because the second pump wave is absent. This configuration is similar to that analysed in [14] and experimentally demonstrated in [15].

The numerical results shown in Figs.3 and 4 fully confirm the analysis from the parametric model. They are obtained from 3D+1 stochastic simulations of the nonlinear propagation equations (2). Numerical integration was performed using a pseudo-spectral (split-step) method in the framework of the Wigner representation, where the field operators are replaced by c-number fields (see e.g. [28]). The input signal field, in the vacuum state, is simulated by Gaussian white noise, while the pump beam is a stationary coherent field with the transverse spatial modulation required by the resonance condition Eq. (6). The two waves forming the dual pump are either plane-waves or have an elliptical Gaussian profile with waists  $500\mu\text{m} \times 200\mu\text{m}$  along the  $x$  and  $y$  axis. The numerical grid size,  $512 \times 256 \times 256$  along the  $x$ ,  $y$  and temporal axis in the plane-wave pump case, was doubled along the  $x$  dimension for the more demanding Gaussian pump case. Figure 3 shows the intensity distributions of the down-converted field after 7 mm of propagation in the NPC, comparing the cases  $r = 0$ ,  $r = 1$  and  $r = -1$ . The bright lines of hot spots at  $q_x = \pm G_x$ , originate from the 4-mode processes that will be discussed in the next section. Incidentally, despite the brightness of the hot-spots, for the chosen gain  $\bar{g} = 0.4\text{mm}^{-1}$  we verified that the pump remains almost undepleted. Fig. 4 plots the logarithm of the mean number of photons sampled on the QPM branches  $\Sigma_0$  and  $\Sigma_{11}$  as a function of  $\bar{g}z$  along the crystal, comparing the use of a single pump versus a dual symmetric pump with the same total energy. The gain enhancement factors  $\gamma$  are estimated by fitting the numerical data, averaged over portions of the corresponding QPM branches far away from the hot-spots, with the prediction of the 2-mode parametric model (11) according to which  $N = \sinh^2(\gamma\bar{g}z)$ . Precisely, they are

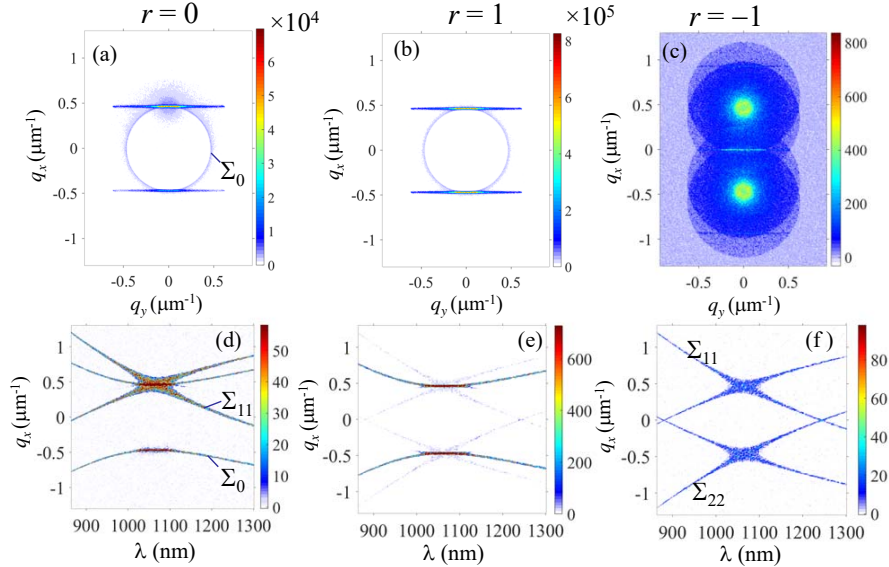


Fig. 3. Photon-number distribution in the  $(q_x, q_y)$ -plane (top) and in the  $(\lambda, q_x)$ -planes (bottom) for a single pump (a,d), two symmetric pumps (b,e) and two antisymmetric pumps (c,f), from numerical simulations of Eqs. (2), in the same NPC of Fig. 2. The pumps are plane-waves,  $\bar{g} = 0.4 \text{ mm}^{-1}$ , and results are shown after 7mm of propagation ( $\bar{g}z = 2.8$ ). In (d,e) the scale was truncated to 1% of the peak value. For a dual symmetric pump the  $\Sigma_0$  branch is significantly more intense than for a single pump of equal energy, while it is absent for antisymmetric pumping. Lines of hot spots at  $q_x = \pm G_x$  are clearly visible in panels (a) and (b).

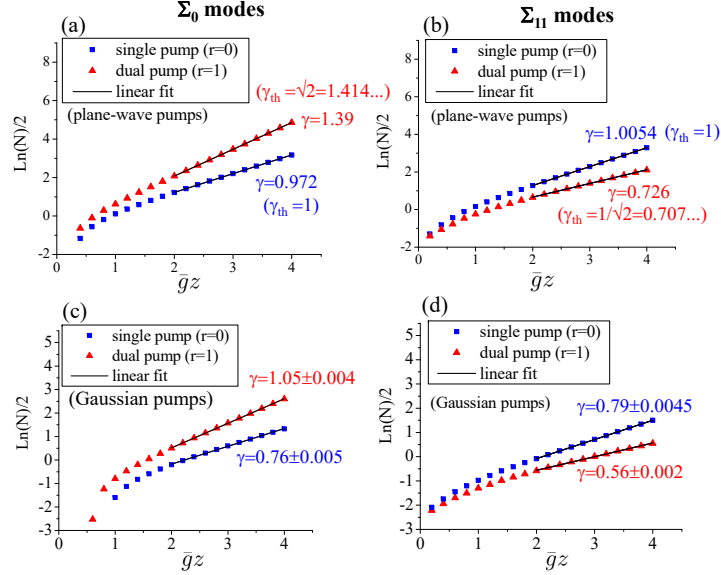


Fig. 4. Comparison between the use of a dual symmetric pump (red triangles) and a single pump (blue squares) with the same energy. The gain enhancement factor  $\gamma$  is evaluated from numerical simulations of Eqs.(2). The results for plane-wave pumps in (a,b) are very close to the  $\gamma_{th}$  predicted by the parametric model [Eq. (13)]. The lower panels (c,d) are obtained for Gaussian pumps, of waists  $500\mu\text{m}$  and  $200\mu\text{m}$  along the  $x$  and  $y$  axis. Other parameters as in Fig. 3

obtained from linear fits of the approximated relation  $\log(N) \approx 2\gamma\bar{g}z$  valid for  $\bar{g}z \gg 1$  (black lines). We verified that a nonlinear fit with the function  $N = \sinh^2(\gamma\bar{g}z)$  provides similar results. For plane-wave pumps, the values of  $\gamma$  inferred in this way are in good agreement with the analytical predictions (13). For Gaussian pumps, the effective gain is significantly reduced in all the cases, but the ratio of the gains for single and dual pumps are roughly preserved. In particular, a dual Gaussian pump provides an enhancement of the gain of the  $\Sigma_0$  modes by a factor  $\sim 1.38$  compared to a single-pump with the same energy, very close to the  $\sqrt{2}$  factor predicted for plane-wave pumps. The number of generated photons on  $\Sigma_0$  at the crystal output, for  $\bar{g}z = 4$ , correspondingly becomes about two orders of magnitude larger.

## 2.2. Shared mode processes

Modes belonging to the interceptions of two QPM surfaces play a special role, since two nonlinear processes concur to the generation of photons, leading to a local enhancement of the gain and to hot spots in the PDC emission [15–18]. Here the complexity is further increased by the dual pumping and by the spatial resonance between the pump and the nonlinear pattern. Similarly to what happens for a pure phase modulation of the pump [14, 15], the spatial resonance produces a 4-mode coupling among shared modes. As we shall see in the following, an intensity modulation of the pump can lead to a boost of the hot-spot intensities, and in general permit to tailor the coupling among the 4 modes.

With a dual pump at spatial resonance with the nonlinear grating [Eq. (6)], the shared modes



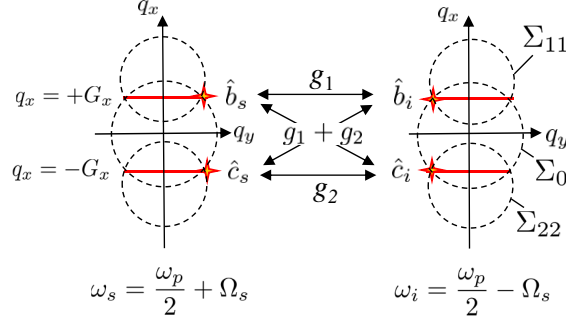


Fig. 5. Example of four-mode coupling process among shared modes at two conjugate frequencies  $\frac{\omega_p}{2} \pm \Omega_s$

are determined by the following equations

$$\mathcal{D}(\vec{w}_s, -\vec{w}_s + 2\vec{\mathcal{G}}_x) = \mathcal{D}(\vec{w}_s, -\vec{w}_s) = 0 \quad \Sigma_0 \cap \Sigma_{11} \quad (14)$$

$$\mathcal{D}(\vec{w}_s, -\vec{w}_s - 2\vec{\mathcal{G}}_x) = \mathcal{D}(\vec{w}_s, -\vec{w}_s) = 0 \quad \Sigma_0 \cap \Sigma_{22} \quad (15)$$

$$\mathcal{D}(\vec{w}_s, -\vec{w}_s + 2\vec{\mathcal{G}}_x) = \mathcal{D}(\vec{w}_s, \vec{w}_s - 2\vec{\mathcal{G}}_x) = 0 \quad \Sigma_{22} \cap \Sigma_{11} \quad (16)$$

We focus here on the intersections between the central surface  $\Sigma_0$  and the two side branches  $\Sigma_{11}$ ,  $\Sigma_{22}$ . As shown in App. A, the first equality in Eqs. (14) and (15) requires that  $q_{sx} = +G_x$  and  $q_{sx} = -G_x$ , respectively. Requiring in addition that QPM is satisfied on these planes, one obtains two continuous lines of shared modes (see the red lines in Fig. 2(a)), that for the chosen phase-matching conditions are characterized by  $q_{sy} = \bar{q}_{sy}(\Omega_s) \simeq \pm \sqrt{k_s k_s''} \Omega_s$ , as can be inferred from Eqs.(8,9). Thus, these shared modes exist also at the degenerate frequency  $\Omega_s = 0$ , where they coincide with the vertexes of the two conical surfaces  $\Sigma_{11}$  and  $\Sigma_{22}$ . Conversely, the shared modes defined by Eq. (16), located at  $q_x = 0$ , exist only away from degeneracy and are much weaker (barely visible in Fig. 3(c)), we shall not discuss them here.

By inspection of Eq. (10), we see that a given shared signal mode  $\vec{w}_s = (+G_x, q_{sy}, \Omega_s)$  couples with  $(-G_x, -q_{sy}, -\Omega_s)$  through both pumps and with  $(G_x, -q_{sy}, -\Omega_s)$  through pump 1 only. The common phase mismatch function vanishes for  $q_{sy} = \bar{q}_{sy}(\Omega)$ . The third term at  $q_x = -3G_x$ , proportional to  $g_2$ , is not phase-matched and can be discarded. A similar reasoning for the other shared mode  $(-G_x, q_{sy}, \Omega_s)$  leads us to conclude that there is a total of four interacting modes, for which we shall use the short hand notation

$$\hat{b}_s := \hat{A}_s(+G_x, q_{sy}, \Omega_s) \quad \hat{b}_i := \hat{A}_s(+G_x, -q_{sy}, -\Omega_s) \quad \text{modes at } q_x = +G_x \quad (17)$$

$$\hat{c}_s := \hat{A}_s(-G_x, q_{sy}, \Omega_s) \quad \hat{c}_i := \hat{A}_s(-G_x, -q_{sy}, -\Omega_s) \quad \text{modes at } q_x = -G_x \quad (18)$$

An example of such a quadruplet of coupled modes is shown in Fig. 5. They satisfy the following

coupled equations

$$\frac{d\hat{b}_s}{dz} = \left[ g_1 \hat{b}_i^\dagger + (g_1 + g_2) \hat{c}_i^\dagger \right] e^{-i\bar{D}z} \quad (19a)$$

$$\frac{d\hat{c}_s}{dz} = \left[ (g_1 + g_2) \hat{b}_i^\dagger + g_2 \hat{c}_i^\dagger \right] e^{-i\bar{D}z} \quad (19b)$$

$$\frac{d\hat{b}_i^\dagger}{dz} = \left[ g_1^* \hat{b}_s + (g_1 + g_2)^* \hat{c}_s \right] e^{i\bar{D}z} \quad (19c)$$

$$\frac{d\hat{c}_i^\dagger}{dz} = \left[ (g_1 + g_2)^* \hat{b}_s + g_2^* \hat{c}_s \right] e^{i\bar{D}z} \quad (19d)$$

where  $\bar{D}$  is the common phase-mismatch of the processes. For  $\bar{D} = 0$ , the eigenvalues of the 4x4 linear system (19) can be readily found as the four real eigenvalues  $\pm\Lambda_+$ ,  $\pm\Lambda_-$ , where

$$\Lambda_{\pm} = \left[ \frac{2|g_1 + g_2| + |g_1| + |g_2|}{2} \pm \frac{1}{2} \sqrt{(|g_1|^2 - |g_2|^2)^2 + 4|g_1 + g_2|^4 + 4[2\text{Im}(g_1 g_2^*)]^2} \right]^{\frac{1}{2}} \\ \rightarrow \frac{\bar{g}}{\sqrt{1+r^2}} \left| \frac{1+r}{2} \pm \frac{1}{2} \sqrt{5(1+r^2) + 6r} \right| = \bar{g} \times \begin{cases} \frac{\sqrt{5}+1}{2} & r = 0 \\ \frac{3}{\sqrt{2}}, \frac{1}{\sqrt{2}} & r = 1 \\ \frac{1}{\sqrt{2}}, \frac{1}{\sqrt{2}} & r = -1 \end{cases} \quad \text{for } r = \frac{g_2}{g_1} \in \mathbb{R} \quad (20)$$

where the second line can be obtained with a little algebra in the simplest case where  $r = \frac{g_2}{g_1}$  is

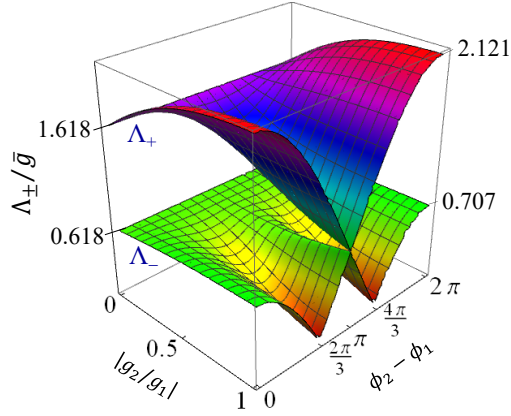


Fig. 6. Eigenvalues  $\Lambda_+$  (upper surface) and  $\Lambda_-$  (lower surface) of the 4-mode propagation equations (19), normalized to  $\bar{g} = \sqrt{|g_1|^2 + |g_2|^2}$  as a function of the ratio  $|r| = \left| \frac{g_2}{g_1} \right|$  of the amplitudes of the two pumps and of their phase difference  $\phi_2 - \phi_1$ .

real, i.e. when the two pumps are either in phase or out of phase by  $\pi$ . These eigenvalues are plotted in Fig. 6, as a function of the ratio  $\left| \frac{g_2}{g_1} \right|$  of the two complex amplitudes of the pumps and of their phase difference  $\phi_2 - \phi_1$ . For a single pump at resonance ( $r = 0$ ) we thus retrieve the results of [14, 15], namely the eigenvalues are  $\bar{g}\Phi$  and  $\bar{g}/\Phi$ , where  $\Phi = \frac{1+\sqrt{5}}{2} = 1.61803\dots$  is the Golden ratio. When a second pump with nonzero amplitude is injected in the crystal, the eigenvalues become modulated with the phase difference between the pumps (Fig. 6(b) and 6(c)). The bigger eigenvalue  $\Lambda_+$  reaches its maximum and minimum values,  $3\bar{g}/\sqrt{2}$  and  $\bar{g}/\sqrt{2}$ , respectively, when the two pumps have equal intensities, either in phase or out of phase by  $\pi$ .

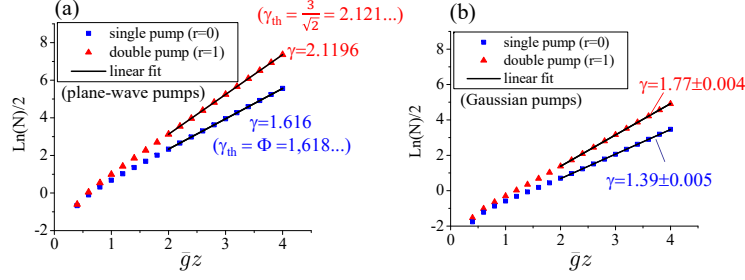


Fig. 7. Evaluation of the gain enhancement factor  $\gamma$  in the hot-spots at  $q_x = \pm G_x$ , from numerical simulations of Eqs.(2). Comparison between the single pump (blue square) and the dual symmetric pump (red triangles), for (a) plane-wave pumps, (b) Gaussian pumps. The crystal and pump parameters are the same as in Fig. 3 and 4.

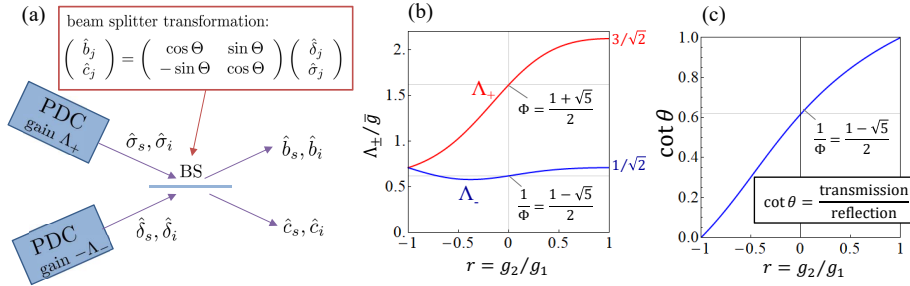


Fig. 8. (a) For  $r = g_2/g_1 \in \mathbb{R}$ , the 4-mode process (19) is equivalent to two independent standard parametric processes of gains  $\Lambda_+$  and  $\Lambda_-$  mixed on a beam splitter. Panel (b) and (c) show the eigenvalues  $\Lambda_{\pm}$  and the ratio between the transmission and reflection coefficients of the beam-splitter as a function of  $r$  respectively.

In the high gain regime  $\bar{g}z \gtrsim 1$ , the number of generated photons is mainly determined by the big eigenvalue, which dominates the exponential rate of growth of the shared modes along the propagation distance. In this regime,  $\Lambda_+/\bar{g}$  can thus be identified with the gain enhancement  $\gamma$  of the hot-spots involved in 4-mode processes compared to standard parametric processes from a single pump with the same energy. Figure 7 provides instead an estimation of the gain enhancement from numerical simulations of the nonlinear propagation equations (2), comparing the use of single and dual pumps, for a given total energy. Again, the values obtained for plane-wave pumps in Fig. 7(a) turn very close to the analytical predictions in Eq. (20) from the simplified 4-mode model, i.e.  $\gamma = \Phi \approx 1.618$  for the single pump ( $r = 0$ ) and  $\gamma = 3/\sqrt{2} \approx 2.121$  for the dual pump ( $r = 1$ ). When considering a Gaussian pump profile as in Fig. 7(b), the effective gains are reduced by about 20%, but the ratio between the dual pump and the single pump values is  $\approx 1.27$ , which is close to the plane-wave pump prediction  $\frac{3}{\sqrt{2}\Phi} \approx 1.31$ . This last result proves that the enhanced conversion efficiency achieved by using a dual pump with a spatial modulation resonant with the NPC grating is a robust feature which affects not only the whole central branch  $\Sigma_0$  but also the hot spots at  $q_{sx} = \pm G_x$ .

In the simplest case  $r \in \mathbb{R}$ , where the eigenvalues are given by Eq. (20), the four-mode equations (19) can be decoupled by means of a unitary transformation which involve  $\hat{b}_s, \hat{c}_s$  and  $\hat{b}_i, \hat{c}_i$

separately

$$\begin{pmatrix} \hat{\delta}_j \\ \hat{\sigma}_j \end{pmatrix} = \begin{pmatrix} \cos \Theta & -\sin \Theta \\ \sin \Theta & \cos \Theta \end{pmatrix} \begin{pmatrix} \hat{b}_j \\ \hat{c}_j \end{pmatrix} \quad j = s, i \quad (21)$$

with  $\cos \Theta = \left( \frac{1}{2} - \frac{1-r}{2\sqrt{5(1+r^2)+6r}} \right)^{1/2}$ ,  $\sin \Theta = \left( \frac{1}{2} + \frac{1-r}{2\sqrt{5(1+r^2)+6r}} \right)^{1/2}$ . The new mode operators  $\hat{\sigma}_j$  satisfy standard 2-mode parametric equations with a gain per unit length  $\Lambda_+$

$$\frac{d\hat{\sigma}_s}{dz} = \Lambda_+ \hat{\sigma}_i^\dagger e^{-i\bar{\mathcal{D}}z} \quad (22)$$

$$\frac{d\hat{\sigma}_i}{dz} = \Lambda_+ \hat{\sigma}_s^\dagger e^{-i\bar{\mathcal{D}}z} \quad (23)$$

while the  $\hat{\delta}_j$  mode operators satisfy similar equations with a comparatively lower gain  $\Lambda_-$

$$\frac{d\hat{\delta}_s}{dz} = -\Lambda_- \hat{\delta}_i^\dagger e^{-i\bar{\mathcal{D}}z} \quad (24)$$

$$\frac{d\hat{\delta}_i}{dz} = -\Lambda_- \hat{\delta}_s^\dagger e^{-i\bar{\mathcal{D}}z} \quad (25)$$

The four-mode coupling process (19) is thus equivalent to the outcome of two independent 2-mode parametric processes of gains  $\Lambda_+$  and  $\Lambda_-$ , followed by an unbalanced beam splitter that mixes the two pairs of twin output modes according to the inverse transformation  $\hat{b}_j = (\cos \Theta)\hat{\sigma}_j + (\sin \Theta)\hat{\delta}_j$ ,  $\hat{c}_j = (\sin \Theta)\hat{\sigma}_j - (\cos \Theta)\hat{\delta}_j$ ,  $j = i, s$ , as shown in Fig.8(a). Both the gains of the two processes and the reflection and transmission coefficients of the beam splitter can be controlled by varying the relative amplitude and phases of the two pumps, as shown in Fig. 8(b) and 8(c). For a single pump  $r = 0$ , we have  $\frac{\sin \Theta}{\cos \Theta} = \Phi$ , and the beam splitter performs a Golden ratio partition of the two pairs of twin beams of gains  $\bar{g}\Phi$  and  $-\bar{g}/\Phi$ , in agreement with the result obtained in [14]. For a dual symmetrical pump  $\cos \Theta = \sin \Theta = 1/\sqrt{2}$ : in this case two twin modes with gains  $3\bar{g}/\sqrt{2}$  and  $\bar{g}/\sqrt{2}$  are generated and then a mixed on a 50:50 beam splitter. For an antisymmetric pump,  $\cos \Theta = 0$ ,  $\sin \Theta = 1$ : indeed in this case  $g_1 + g_2 = 0$  and the four-mode process (19) uncouples trivially into two standard parametric processes with equal gain  $\bar{g}/\sqrt{2}$ , which populate only the side branches  $\Sigma_{11}$  and  $\Sigma_{22}$ .

### 3. Conclusions

This work investigated parametric down-conversion in a hexagonally poled nonlinear photonic crystal pumped by two tilted pumps, forming a spatial transverse pattern. When the pump pattern matches the periodicity of the nonlinear grating, we have shown the existence of a two-fold degenerate QPM branch of spatio-temporal modes (a surface  $\Sigma_0$  in the 3D Fourier space), where photon pairs are generated from both pump modes, and are quasi-phase-matched by both fundamental vectors of the 2D nonlinear grating.

In contrast, quasi-phasematching in nonlinear photonic crystals in the standard single pump configuration generally involves only one lattice vector at a time, except for restricted families of modes of lower dimensionality, the shared modes, which lie at the interceptions of different QPM branches. The two-fold degeneracy of the  $\Sigma_0$  branch is thus a distinctive feature of the spatial resonance of the dual pump with the nonlinear grating. As a consequence, its gain per unit propagation length is proportional to the sum  $|\alpha_1 + \alpha_2|$  of the complex amplitudes of the two pumps, and can be controlled by varying their relative amplitudes and phases. For two symmetric pumps ( $\alpha_1 = \alpha_2$ ), the down-conversion process is strongly enforced by the

pump transverse modulation  $\propto \cos(G_x x)$  which oscillates in phase with the nonlinear lattice. Conversely, down-conversion is inhibited for two anti-symmetric pumps  $\alpha_2 = -\alpha_1$ , because the pump modulation  $\propto \sin(G_x x)$  is in quadrature of phase with the nonlinear lattice.

Specifically, when comparing the use of a dual symmetric pump and a single pump with the same total energy, the conversion efficiency on the  $\Sigma_0$  branch simply doubles in the purely spontaneous PDC regime. However in the stimulated regime, where the number of generated photon pairs grows exponentially along the crystal, the  $\sqrt{2}$  increase of the gain per unit length leads to a huge increase of the efficiency.

We also analysed the four-mode coupling characterizing the resonant condition, and we showed that is equivalent to two independent parametric processes of different gain generating each a pair of twin beams, followed by an unbalanced beam splitter that mixes the two outcomes with transmission and reflection coefficients related to the pump amplitudes. The present work is mainly devoted to the classical aspects; the quantum aspects will be discussed in a related work [23], showing how the control of intensities and phases of the dual pumps may be used to tailor the quadri-partite entanglement of the shared modes.

#### 4. Funding

This is supported by the Italian 'Ministero dell' Istruzione, dell'Università e della Ricerca' (MIUR).

#### A. QPM surfaces and shared modes

In this appendix we provide analytical expressions for the QPM surfaces and for the shared modes at the interceptions of these surfaces. We consider the paraxial approximation with the longitudinal components of the signal wave-vector given by

$$k_{sz}(\vec{w}_s) \approx k_s(\Omega_s) - \frac{q_s^2}{2k_s(\Omega_s)}, \quad (1)$$

Noticing that the phase-matching functions which determine the various QPM surfaces (5a)-(5d) are distinguished only by the resultant of the pump and lattice transverse wave-vectors:  $\vec{\mathcal{R}}_{11} = (q_{0p} + G_x)\vec{e}_x$ ;  $\vec{\mathcal{R}}_{12} = (q_{0p} - G_x)\vec{e}_x$ ;  $\vec{\mathcal{R}}_{21} = (-q_{0p} + G_x)\vec{e}_x$ ;  $\vec{\mathcal{R}}_{22} = (-q_{0p} - G_x)\vec{e}_x$ , we can write such functions as

$$\mathcal{D}(\vec{w}_s, -\vec{w}_s + \vec{\mathcal{R}}_{lm}) = k_{sz}(\vec{w}_s) + k_{sz}(-\vec{w}_s + \vec{\mathcal{R}}_{lm}) - k_{pz}(\vec{w}_{0p}) + G_z \quad (2)$$

$$\begin{aligned} &\simeq k_s(\Omega) + k_s(-\Omega_s) - k_{pz} + G_z - \frac{|\vec{\mathcal{R}}_{lm}|^2}{2(k_s(\Omega_s) + k_s(-\Omega_s))} \\ &- \frac{k_s(\Omega_s) + k_s(-\Omega_s)}{2k_s(-\Omega_s)k_s(-\Omega)} \left| \vec{q} - \frac{k_s(\Omega_s)}{k_s(\Omega_s) + k_s(-\Omega_s)} \vec{\mathcal{R}}_{lm} \right|^2, \quad (l, m = 1, 2) \end{aligned} \quad (3)$$

where  $k_{pz}$  is the common z-component of the wavevectors of the two monochromatic pumps of wavelength  $\lambda_p$  and transverse wavevector  $\pm q_{0p}\vec{e}_x$ . According to this result, at a given signal frequency  $\Omega_s$ , the down-converted field is generated provided that

$$\begin{aligned} D_0(\Omega_s) &= k_s(\Omega) + k_s(-\Omega_s) - k_{pz} + G_z - \frac{|\vec{\mathcal{R}}_{lm}|^2}{2(k_s(\Omega_s) + k_s(-\Omega_s))} \\ &\approx 2k_s - k_{pz} + G_z - \frac{|\vec{\mathcal{R}}_{lm}|^2}{4k_s} + k_s''\Omega_s^2 \geq 0 \end{aligned} \quad (4)$$

where in the second line we made a Taylor series expansion up to second order in  $\Omega_s$ , valid not too far from degeneracy, and  $k_s'' = \frac{d^2 k_s}{d\Omega_s^2} \Big|_{\Omega_s=0}$ . Provided that the inequality (4) is satisfied, then

the QPM signal modes lie on circumferences in the  $(q_x, q_y)$  plane, whose centers

$$\vec{q}_{lm} = \frac{k_s(\Omega)}{k_s(\Omega) + k_s(-\Omega)} \vec{\mathcal{R}}_{lm} \approx \frac{\vec{\mathcal{R}}_{lm}}{2} \quad (5)$$

are distributed along the  $q_x$ -axis, and of radial apertures

$$Q_{lm} = \left[ \frac{2k_s(\Omega)k_s(-\Omega)}{k_s(\Omega) + k_s(-\Omega)} D_0(\Omega_s) \right]^{\frac{1}{2}} \approx \sqrt{k_s D_0(\Omega_s)} \quad (6)$$

In general, in the nonresonant case when  $q_{op} \neq G_x$ , one has four distinct QPM branches, corresponding to the four possible resultants of the pump and lattice transverse wavevectors. Figure. 9 shows an example of such four QPM branches, from a numerical simulation of the evolution equations, for a dual symmetric pump with  $q_{op} = 1.2G_x$ .

In the resonant case the two surfaces  $\Sigma_{12}$  and  $\Sigma_{21}$  degenerate into a single surface  $\Sigma_0$  corresponding to a transverse resultant  $\vec{\mathcal{R}}_{12} = \vec{\mathcal{R}}_{21} = 0$ . The other two QPM branches are characterized by the resultants  $\vec{\mathcal{R}}_{11} = -\vec{\mathcal{R}}_{22} = 2G_x \vec{e}_x$ . We have chosen the poling period in such a way that

$$2k_s - k_{pz} + G_z - \frac{|2G_x|^2}{4k_s} = 0 \quad (7)$$

Taking into account Eqs.(4)-(6),  $\Sigma_{11}$  and  $\Sigma_{22}$  are then well approximated by two bi-conical surfaces having their vertexes at  $q_x = \pm G_x$ ,  $q_y = 0$ ,  $\Omega = 0$ :

$$\Sigma_{11} : |\vec{q}_s - G_x \vec{e}_x| \approx \sqrt{k_s k_s''} |\Omega_s|, \quad (8)$$

$$\Sigma_{22} : |\vec{q}_s + G_x \vec{e}_x| \approx \sqrt{k_s k_s''} |\Omega_s|, \quad (9)$$

which in the plane  $(\Omega_s, q_x)$  appear as two X's, vertically displaced along  $q_x$  of an amount  $2G_x$  (See Fig 2b). Within the same approximation,  $\Sigma_0$  is given by

$$\Sigma_0 : |\vec{q}_s| \approx (G_x^2 + k_s k_s'' \Omega_s^2)^{1/2}, \quad (10)$$

which appears like a widely opened tube centered at  $\vec{q} = 0$ , intersecting the vertexes  $\pm G_x \vec{e}_x$  of the two conical surfaces as shown in Fig. 2(a).

Let us now determine the interceptions of the QPM surfaces, corresponding to the shared modes. In general, the QPM modes shared by two surfaces  $\Sigma_{lm}$  and  $\Sigma_{pq}$  lie on a curve defined by:

$$\Sigma_{lm} \cap \Sigma_{pq} : \mathcal{D}(\vec{w}_s, -\vec{w}_s + \vec{\mathcal{R}}_{lm}) = \mathcal{D}(\vec{w}_s, -\vec{w}_s + \vec{\mathcal{R}}_{pq}) = 0, \quad (11)$$

Taking into account Eq. (2), the first equality in Eq. (11) implies that

$$k_{sz}(-\vec{w}_s + \vec{\mathcal{R}}_{lm}) = k_{sz}(-\vec{w}_s + \vec{\mathcal{R}}_{pq}) \rightarrow q_{sx} = \frac{\vec{\mathcal{R}}_{lm} + \vec{\mathcal{R}}_{pq}}{2} \quad (12)$$

Then for example the QPM modes shared by  $\Sigma_{11}$  and  $\Sigma_{12}$  are characterized by the  $x$ -component of the wave vector  $q_{sx} = q_{op}$ , while those shared by  $\Sigma_{11}$  and  $\Sigma_{21}$  are located at  $q_{sx} = G_x$ . For reasons of symmetry the modes shared by  $\Sigma_{22}$  and  $\Sigma_{21}$  are located at  $q_{sx} = -q_{op}$ , while those shared by  $\Sigma_{22}$  and  $\Sigma_{12}$  have  $q_{sx} = -G_x$ . In the plane  $(q_x, q_y)$  the shared modes form four straight lines at  $q_x = \pm q_{op}$ , and  $q_x = \pm G_x$ , as shown by the numerical simulations in Fig.9(a). The corresponding hot spots have however a much lower intensity than in the resonant case (see Fig. 3(b)). At spatial resonance  $q_{op} = \pm G_x$ , the four lines of shared modes merge into two ones at  $q_{sx} = \pm G_x$ . In the 3D Fourier space, they merge into the two curves of equations  $q_{sx} = \pm G_x$ ;  $q_{sy} = \vec{q}_{sy}(\Omega) = \pm \sqrt{k_s k_s''} |\Omega_s|$  (red lines in Fig. 2(a)).

The remaining shared modes belonging to  $\Sigma_{11} \cap \Sigma_{22}$  and  $\Sigma_{12} \cap \Sigma_{21}$  are located at  $q_{sx} = 0$  plane, generally on different curves. We shall not take these modes into consideration as they lie far from degeneracy.

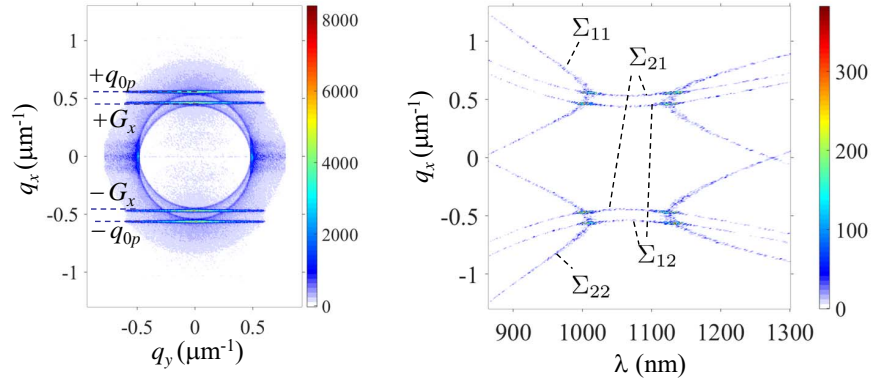


Fig. 9. Results of simulations away from resonance, for two symmetric pumps with  $q_{0p} = 1.2 G_x$ . (a) Intensity distribution in the  $(q_x, q_y)$  plane, showing four lines of hot spots at  $q_x = \pm q_{0p}$  and  $q_x = \pm G_x$ . (b) Intensity distribution in the  $(\lambda, q_x)$  plane ( $q_y = 0$ ). Other parameters as in Fig. 3.

## References

1. V. Berger, "Nonlinear photonic crystals," *Phys. Rev. Lett.* **81**, 4136–4139 (1998).
2. N. G. R. Broderick, G. W. Ross, H. L. Offerhaus, D. J. Richardson, and D. C. Hanna, "Hexagonally poled Lithium Niobate: A two-dimensional nonlinear photonic crystal," *Phys. Rev. Lett.* **84**, 4345–4348 (2000).
3. S. Saltiel and Y. S. Kivshar, "Phase matching in nonlinear  $\chi^{(2)}$  photonic crystals," *Opt. Lett.* **25**, 1204–1206 (2000).
4. K. Gallo, A. Pasquazi, S. Stivala, and G. Assanto, "Parametric solitons in two-dimensional lattices of purely nonlinear origin," *Phys. Rev. Lett.* **100**, 053901 (2008).
5. K. Stensson, G. Björk, and K. Gallo, "Green-pumped parametric downconversion in hexagonally poled  $\text{MgO:LiTaO}_3$ ," in *Advanced Solid State Lasers*, (Optical Society of America, 2014), p. ATu3A.5.
6. M. Lazoul, A. Boudrioua, L.-M. Simohamed, and L.-H. Peng, "Multi-resonant optical parametric oscillator based on 2D-PPLT nonlinear photonic crystal," *Opt. Lett.* **40**, 1861–1864 (2015).
7. Z. Yellas, M. W. Lee, R. Kremer, K.-H. Chang, M. R. Beghou, L.-H. Peng, and A. Boudrioua, "Multiwavelength generation from multi-nonlinear optical process in a 2D PPLT," *Opt. Express* **25**, 30253–30258 (2017).
8. H. Chikh-Touami, R. Kremer, H.-J. Lee, M. Lee, L.-H. Peng, and A. Boudrioua, "Experimental investigation of optical parametric generation enhancement in nonlinear photonic crystal of  $\text{LiTaO}_3$ ," *J. Opt.* **19**, 065503 (2017).
9. H. Chikh-Touami, R. Kremer, H.-J. Lee, M. Lee, L.-H. Peng, and A. Boudrioua, "Shared optical parametric generation interactions in square lattice nonlinear photonic crystals," *Appl. Phys. B: Lasers Opt.* **123**, 113 (2017).
10. H. Jin, P. Xu, X. W. Luo, H. Y. Leng, Y. X. Gong, W. J. Yu, M. L. Zhong, G. Zhao, and S. N. Zhu, "Compact engineering of path-entangled sources from a monolithic quadratic nonlinear photonic crystal," *Phys. Rev. Lett.* **111**, 023603 (2013).
11. Y.-X. Gong, P. Xu, Y. F. Bai, J. Yang, H. Y. Leng, Z. D. Xie, and S. N. Zhu, "Multiphoton path-entanglement generation by concurrent parametric down-conversion in a single  $\chi^{(2)}$  nonlinear photonic crystal," *Phys. Rev. A* **86**, 023835 (2012).
12. E. Megidish, A. Halevy, H. S. Eisenberg, A. Ganany-Padovicz, N. Habshoosh, and A. Arie, "Compact 2D nonlinear photonic crystal source of beamlike path entangled photons," *Opt. Express* **21**, 6689–6696 (2013).
13. Y.-X. Gong, S. Zhang, P. Xu, and S. N. Zhu, "Scheme for generating distillation-favorable continuous-variable entanglement via three concurrent parametric down-conversions in a single  $\chi^{(2)}$  nonlinear photonic crystal," *Opt. Express* **24**, 6402–6412 (2016).
14. A. Gatti, E. Brambilla, K. Gallo, and O. Jedrkiewicz, "Golden ratio entanglement in hexagonally poled nonlinear crystals," *Phys. Rev. A* **98** (2018).
15. O. Jedrkiewicz, A. Gatti, E. Brambilla, M. Levenius, G. Tamosauskas, and K. Gallo, "Golden ratio gain enhancement in coherently coupled parametric processes," *Sci. Rep.* **8**, 11616 (2018).
16. H.-C. Liu and A. H. Kung, "Substantial gain enhancement for optical parametric amplification and oscillation in two-dimensional  $\chi^{(2)}$  nonlinear photonic crystals," *Opt. Express* **16**, 9714–9725 (2008).
17. M. Levenius, V. Pasiskevicius, and K. Gallo, "Angular degrees of freedom in twin-beam parametric down-conversion," *Appl. Phys. Lett.* **101**, 121114– (2012).
18. L. Chen, P. Xu, Y. F. Bai, X. W. Luo, M. L. Zhong, M. Dai, M. H. Lu, and S. N. Zhu, "Concurrent optical parametric down-conversion in  $\chi^{(2)}$  nonlinear photonic crystals," *Opt. Express* **22**, 13164–13169 (2014).
19. M. Conforti, F. Baronio, M. Levenius, and K. Gallo, "Broadband parametric processes in  $\chi^{(2)}$  nonlinear photonic

- crystals,” *Opt. Lett.* **39**, 3457–3460 (2014).
20. R. Danielius, P. Di Trapani, A. Dubietis, A. Piskarskas, D. Podenas, and G. P. Banfi, “Self-diffraction through cascaded second-order frequency-mixing effects in  $\beta$ -barium borate,” *Opt. Lett.* **18**, 574–576 (1993).
  21. M. Tiihonen and V. Pasiskevicius, “Two-dimensional quasi-phase-matched multiple-cascaded four-wave mixing in periodically poled ktiopo<sub>4</sub>,” *Opt. Lett.* **31**, 3324–3326 (2006).
  22. A. Arie, N. Habshoosh, and A. Bahabad, “Quasi phase matching in two-dimensional nonlinear photonic crystals,” *Opt. Quant. Electron.* **39**, 361–375 (2007).
  23. A. Gatti and E. Brambilla, “Engineering multipartite entanglement in nonlinear photonic crystals,” Preprint.
  24. H. H. Lim, S. Kurimura, T. Katagai, and I. Shoji, “Temperature-dependent sellmeier equation for refractive index of 1.0 mol % Mg-doped stoichiometric lithium tantalate,” *Jpn. J. Appl. Phys.* **52**, 032601 (2013).
  25. A. Gatti, R. Zambrini, M. San Miguel, and L. A. Lugiato, “Multiphoton multimode polarization entanglement in parametric down-conversion,” *Phys. Rev. A* **68**, 053807 (2003).
  26. E. Brambilla, O. Jedrkiewicz, L. A. Lugiato, and A. Gatti, “Disclosing the spatiotemporal structure of parametric down-conversion entanglement through frequency up-conversion,” *Phys. Rev. A* **85**, 063834 (2012).
  27. K. Moutzouris, G. Hloupis, I. Stavrakas, D. Triantis, and M.-H. Chou, “Temperature-dependent visible to near-infrared optical properties of 8 mol% Mg-doped lithium tantalate,” *Opt. Mater. Express* **1**, 458–465 (2011).
  28. M. J. Werner and P. D. Drummond, “Pulsed quadrature-phase squeezing of solitary waves in  $\chi^{(2)}$  parametric waveguides,” *Phys. Rev. A* **56**, 1508–1518 (1997).